

Iranian Journal of Oil & Gas Science and Technology, Vol. 12 (2023), No. 1, pp. 01–14  
http://ijogst.put.ac.ir

## Detecting Heavy Bitumen Contaminations Using Corrected Rock-Eval Pyrolysis Data

M. Hemmati<sup>1</sup> and Y. Ahmadi<sup>2\*</sup>

<sup>1</sup> MS Student, School of Geology, College of Science, University of Tehran, Tehran, Iran.

<sup>2</sup> Assistant Professor, Chemical and Petroleum Engineering Department, Ilam University, P.O. Box 69315/516, Ilam, Iran.

### Highlights

- Application of the petroleum potential ( $S_2$ ) versus total organic carbon (TOC) graph in detecting in situ bitumen contamination;
- Evaluating the accuracy of geochemistry data obtained from the Rock-Eval pyrolysis apparatus;
- The  $y$ -intercept in the graph of  $S_2$  versus TOC;
- Determining depositional system tracts using the graph of  $S_2$  versus TOC.

Received: June 21, 2021; revised: August 06, 2021; accepted: August 20, 2021

### Abstract

Rock-Eval pyrolysis is a thermal method petroleum geologists use to evaluate source rock characteristics and obtain geochemistry parameters. However, there are misconceptions and misuses in exceptional cases that could lead to erroneous conclusions after using the Rock-Eval pyrolysis data to evaluate the properties of organic matter. However, a cross-plot of petroleum potential ( $S_2$ ) versus total organic carbon (TOC) is a useful tool for solving issues and checking the accuracy of the geochemistry parameters. The graph provides the correction criteria for the  $S_2$ , hydrogen index (HI), and kerogen types. As well as the graph measures the adsorption of hydrocarbon by the mineral matrix. In addition, this article demonstrates a manner based on the data plot of  $S_2$  versus TOC to detect bitumen or hydrocarbon contaminations. Based on our knowledge about the Garau formation as a possible source rock in the petroleum geology of Iran, a geochemistry study by Rock-Eval VI pyrolysis and LECO carbon analyzer has been conducted on many rock samples collected from different outcrops in the Lurestan province, Aligudarz region, from southwest of Iran, High Zagros. Plotting the data on a cross plot of  $S_2$  versus TOC, drawing the regression line, and finding the regression equation are the best methods for determining the actual values of  $S_2$  and HI parameters and bitumen/hydrocarbon contamination. Contamination creates a  $y$ -intercept in the graph of  $S_2$  versus TOC, making geochemistry data unreliable in two study locations. The  $S_2$  and HI data unrealistically increase, while the  $T_{\max}$  values decline and reduce the thermal maturity of the organic matter from its actual status. The  $y$ -intercept of the graphs is removed, and the corresponding values are subtracted from the HI and  $S_2$  to skip the effect of contamination and obtain the actual geochemistry parameters. The cause of contamination in the Garau formation is the adhesion of heavy bitumen to organic facies due to the covalent bonds between carbon and hydrogen ions.

**Keywords:** Rock-Eval pyrolysis, heavy bitumen contamination, geochemistry, sedimentary system tracts

\* Corresponding author:

Email: yaser.ahmadi@ilam.ac.ir

**How to cite this article**

Hemmati .M and Ahmadi. Y, *Detecting Heavy Bitumen Contaminations Using Corrected Rock-Eval Pyrolysis Data*, Iran J. Oil Gas Sci. Technol., Vol. 12, No. 1, p. 01–14, 2023. DOI: <http://dx.doi.org/10.22050/ijogst.2021.290550.1598>

## 1. Introduction

Petroleum geochemistry is an established science that improves exploration and production efficiency, and it has been characterized as a mature science for increasing the chances of success in oil exploration (Bordenave, 1993; Miller, 1995; Peters and Fowler, 2002). Petroleum geologists should check the accuracy of the data before interpretation, and this fact decreases the risk of projects and the possibility of dealing with unexpected cases and even reduces irreparable costs. Obtaining geochemistry data by the Rock-Eval pyrolysis is a quick, low-cost, and most applied technique for evaluating the petroleum generation potential of source rocks. It provides information on the quantity, type, and thermal maturity of the associated organic matter (Espitalie, 1977; Peters, 1986). The petroleum potential of source rocks is related to their organic carbon content, and the total organic carbon (TOC) analysis is the first screening analysis method for evaluating the general hydrocarbon potential (Jarvie, 1991; Tissot and Welte, 1984).

In the cross-plots of petroleum potential ( $S_2$ ) versus TOC, there is a linear function between TOC,  $S_2$ , and hydrogen index (HI) values (Clayton and Ryder, 1984; Langford and Valleron, 1990). The hydrogen index derived from the regression line in such a cross-plot can measure the average HI of the organic matter that is pyrolysable (Dahl et al., 2004; Maky et al., 2010). When the regression line is not intersecting at the origin of the graph, the total HI, according to the slope of the curve (regression line), is different from the arithmetic mean of the HI. In cases where  $y_0 = 0$  and the regression line intersects the origin, the HI values derived from the arithmetic mean or the slope of the curve are close to each other (Dahl et al., 2004). In other cases, when the regression line does not pass through the origin of the graph, there is an  $x$ -intercept or  $y$ -intercept.

Previous reports reveal that the Garau formation is a potential and practical source of rock in the southwest of Iran (Bordenave and Burwood, 1990; Bordenave and Hegre, 2010), and most probably it charged limited reservoirs in that region (Bordenave and Hegre, 2005). Based on the need for further geochemistry studies about the Garau formation, especially its hydrocarbon-generation potential, in the current study, the geochemistry parameters are obtained by the Rock-Eval apparatus, and the LECO technique does the carbon analysis. In this research, geochemistry analyses are applied to five outcrop rock samples of the Garau formation, and the accuracy of geochemistry data is evaluated to create a criterion accuracy of the geochemistry data.

## 2. Geological setting and stratigraphy

The Zagros orogenic belt is limited to the Zagros reverse fault in the northeast and to the Dezful embayment in the southeast, where the Lurestan depression is located in the northwest part of it. Many reservoirs and source rocks have been detected in this region, and the Garau formation is one of the most effective source rocks (Bordenave and Burwood, 1990). The Garau formation's type section has been defined on the southwestern flank of Kabir Kuh in southwestern Lurestan near the Qaleh Darreh village. The Garau formation underlies the Sarvak formation in its type section, and from the Lurestan zone toward Dezful embayment and Fars's basin, this formation gradually passes into the carbonate platform strata of the upper Khami group. Its lithological and geochemical characteristics vary in other regions (Bordenave and Burwood, 1990). The formation's age in its type section relates to the Neocomian to Coniacian (Wynd, 1965). However, the age of the upper part of this formation is also

attributed to upper Toronian (Alavi, 2004; Bordenave and Burwood, 1990) or Aptian, Albian (Al-Husseini and Moujahed, 2000). These differences seem to be related to the location of the study. The Garau formation comprises low energy facies locally pyritic, argillaceous lime micritic limestone (mudstone), and dark gray to black, organic matter-rich bioclastic shale (Alavi, 2004). The Garau formation overlies the Gotnia evaporites in the Lurestan basin, deposited in deeper parts of a continental shelf, and is the time equivalent of the Gadvan, Kazhdumi, and Dariyan formations in other regions of Iran (Alavi, 2004; Ghazban and Motiei, 2007). The thickness of the formation is about 624 m in its type section (Ghazban and Motiei, 2007). In the study area, the Garau intervals are characterized by sizeable lateral variation in thickness, showing at some localities' pinch and swell structures. Figure 1 shows the study area with its tectonic elements, and Figure 2 is a schematic stratigraphy chart of the Lurestan basin in the Zagros orogeny belt.

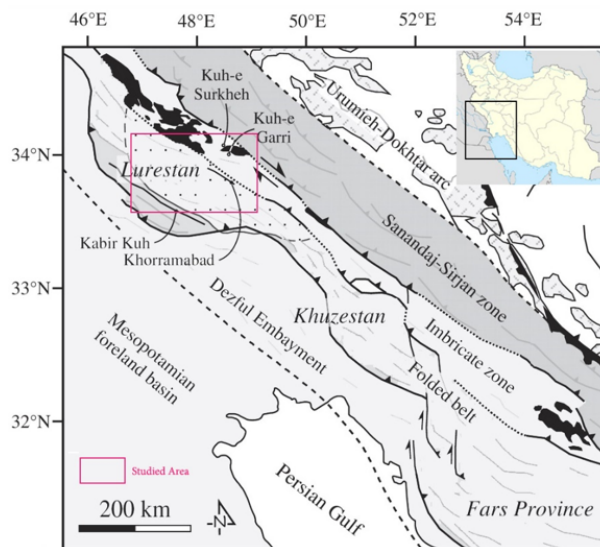


**Figure 1**

The structural setting of the Zagros fold-thrust-belt showing the study area situations (Homke et al., 2009).

Schematic Stratigraphy of SW Iran (Lurestan)			
Age	Formation	Lithology	Description
Lower Cretaceous	Garau	[Pattern: brick-like]	Mainly argillaceous limestone with black shales
		[Pattern: solid black]	
Upper Jurassic	Gotnia	[Pattern: dotted]	Altered limestone with anhydrite intercalation
	Najmeh	[Pattern: wavy]	Mainly oolitic limestone
Middle Jurassic	Sargelu	[Pattern: brick-like]	Black radiolaria bearing shales and argillaceous carbonates

**Figure 2**

The schematic stratigraphy of the Lurestan basin (modified after Motiei, 1993).

### 3. Materials and methods

#### 3.1. Sampling

In this study, 123 outcrop rock samples have been collected from the organic matter-rich facies of the Garau formation in five locations (A, B, C, D, and E) in Lorestan province, southwest of Iran, High Zagros. In each location, the samples were systematically collected from the base to the top of the intervals, with a vertical sampling distance of 1.5 m. The possible surface alterations were eliminated before use. The sample was primarily treated with HCl and HF solutions to remove carbonate and silicates so as to directly measure TOC using the LECO method (Hunt, 1996; Tyson, 1995).

#### 3.2. LECO carbon analyzer

In the LECO method, the organic carbon is combusted without the intervention of mineral carbon (e.g., carbon in argillaceous limestone or clay samples), so determining total carbon by the LECO method is better than calculation by Rock-Eval pyrolysis, especially for carbon-rich samples. Hence, samples were first crushed and then acid treated according to the abovementioned method. After that, they combusted at about 1000 °C using a high-frequency induction furnace in an oxygen atmosphere using a LECO CR-412 apparatus. Next, the carbon contained in the kerogen was converted to CO and CO<sub>2</sub>. Finally, the evolved carbons were measured in an infrared cell and converted to TOC (Bernard, 2010; Peters, 1986).

#### 3.3. Rock-Eval pyrolysis

The Rock-Eval VI analysis was performed to obtain geochemical parameters. The Rock-Eval pyrolysis uses temperature-programmed heating of a small amount of rock (100 mg) in an oxygen-free atmosphere (helium or nitrogen). The generated liquid hydrocarbons are recorded in peaks as S<sub>1</sub> (free hydrocarbon; mg HC/g rock), S<sub>2</sub> (cracked hydrocarbon; mg HC/g rock), S<sub>3</sub> (derived from oxygen-containing organic molecules; mg CO<sub>2</sub>/g rock) (Espitalié, 1985a, 1985b; Espitalié et al., 1977). Other necessary measurements include  $T_{max}$ , hydrogen index, and oxygen index (OI) (Peters, 1986).

#### 3.4. The S<sub>2</sub> versus TOC diagram

Plotting the data on the graph of S<sub>2</sub> versus TOC, and drawing the regression line, is a useful tool to determine real geochemistry parameters, such as HI, production index ( $PI = S_1/S_1 + S_2$ ), kerogen type, and main expelled products. Another important usage of the cross-plot is to detect mineral matrix effect and bitumen or hydrocarbon contamination, according to the  $x$ -intercept and  $y$ -intercept created on the graph, respectively (Langford and Valleron, 1990; Dahl et al., 2004). As the data must first be plotted, the regression line should be drawn to acquire the line equation. The line equation is a first-order equation such as Equations (1) and (2) (Thomas et al., 2016):

$$y = mx \pm y_0 \quad (1)$$

$$S_2 = mTOC \pm y_0 \quad (2)$$

The slope of the regression line ( $m$ ) equals  $\tan\alpha$ , which represents the HI. As well as, the constant ( $y_0$ ) is the intersection from the origin that is the representative of underestimation ( $-y_0$ ) and overestimation ( $+y_0$ ) in the S<sub>2</sub> or HI when the  $x$ -intercept and  $y$ -intercept are induced, respectively. On the one hand, the high organic matter contents in the source rock yield low products; on the contrary, the low organic matter contents produce higher products. In other words, when  $y_0 = -b$ , there is an  $x$ -intercept; when  $y_0 = +b$ , there is a  $y$ -intercept. The intersection from the  $x$ -axis represents the average amount of inert or



Location name	S <sub>1</sub> (mg HC/g rock)	S <sub>2</sub> (mg HC/g rock)	S <sub>3</sub> (mg CO <sub>2</sub> /g rock)	TOC (wt %)	T <sub>max</sub> (°C)	S <sub>2</sub> /S <sub>3</sub>	HI (mg HC/gr TOC)	OI (mg CO <sub>2</sub> /g TOC)	PP (mg HC/gr TOC)	PI
B	0.5	38.4	0.8	7.1	433.5	30.6	449.3	26.8	38.9	0.02
Average										
Maximum	3.3	139.6	2.1	24.2	438.0	77.5	621.0	57.0	142.8	0.05
Minimum	0.0	1.4	0.3	0.6	431.0	4.7	213.0	7.0	1.4	0.00
C	1.7	90.5	1.7	16.4	431.8	61.9	555.2	10.6	92.2	0.02
Average										
Maximum	2.5	111.6	3.5	19.4	436.0	106.2	611.0	20.0	114.1	0.03
Minimum	0.6	66.0	1.0	10.8	429.0	23.4	479.0	5.0	66.7	0.01
D	1.0	67.0	1.1	12.4	431.0	61.9	478.7	39.2	68.0	0.02
Average										
Maximum	2.1	115.9	2.7	21.4	436.0	126.4	576.0	258.0	117.3	0.06
Minimum	0.0	0.3	0.6	0.3	427.0	0.4	106.0	4.0	0.4	0.01
E	2.1	82.6	1.4	15.5	431.0	73.2	497.0	14.6	84.7	0.03
Average										
Maximum	4.6	140.2	2.8	26.4	441.0	222.5	667.0	56.0	144.8	0.18
Minimum	0.1	1.2	0.5	1.3	423.0	1.7	93.0	2.0	1.4	0.01

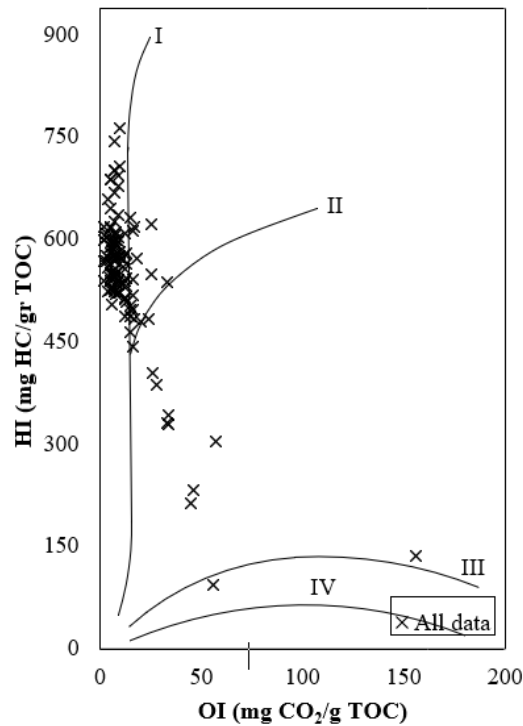


**Figure 3**

The cross-plots of HI versus OI, showing the presence of kerogen types I, I/II, and II (Hunt, 1996).

### 4.2. The S<sub>2</sub> versus TOC diagram

The cross-plot of HI versus TOC reveals indigenous relations between products and organic matter contents (Figure 4). Thus, the HI increases with an increase in the TOC. The regression line demonstrates how the HI increases with increasing the TOC. Moreover, based on the almost similar trend between HI and TOC data, the products mainly come from the exact origin. However, the figure shows an irrational relationship between HI versus TOC for many samples, so the high HI is obtained from the low TOC contents, implying high bitumen/hydrocarbon produced from lower organic matter contents. On the other hand, the regression line in the S<sub>2</sub> versus TOC cross-plot in the A and C location samples does not pass through the origin (Figure 5). Another irrational situation is established in the locations of B, D, and E, where due to the mineral matrix effect in adsorbing hydrocarbons, the lower HI has derived from the higher TOC (Langford and Valleron, 1990; Dahl et al., 2004).

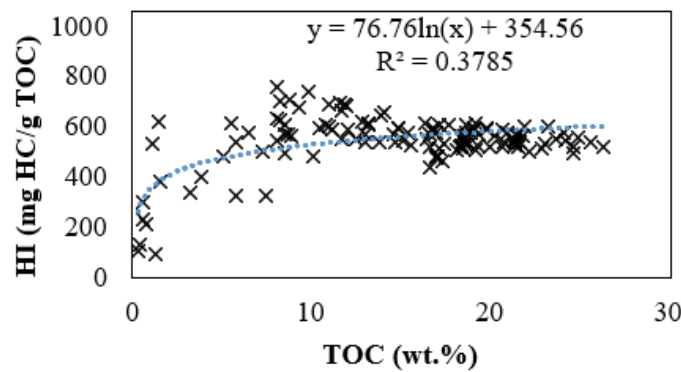
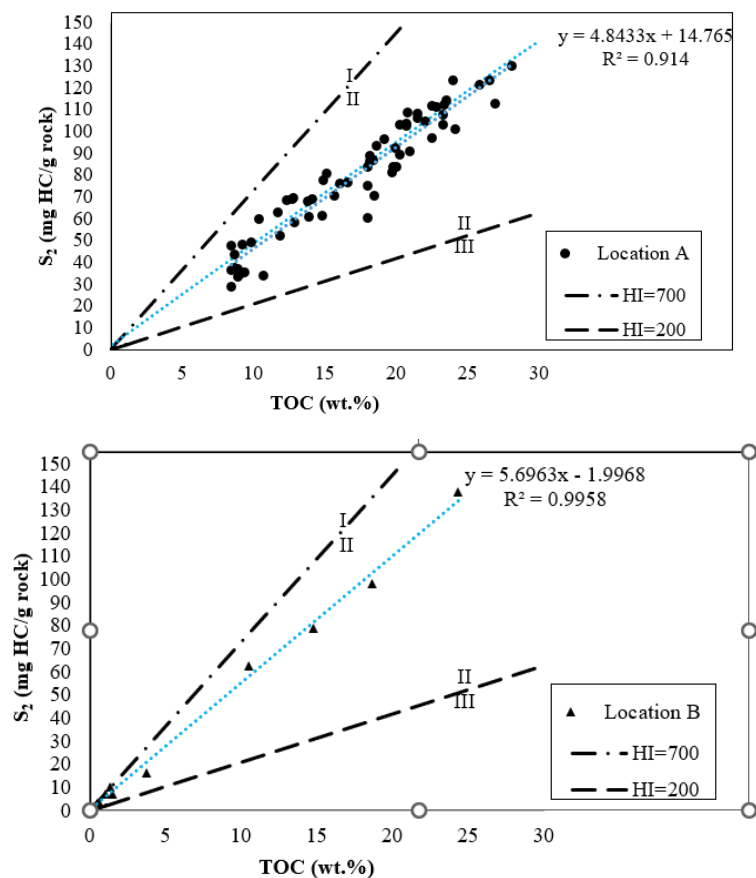
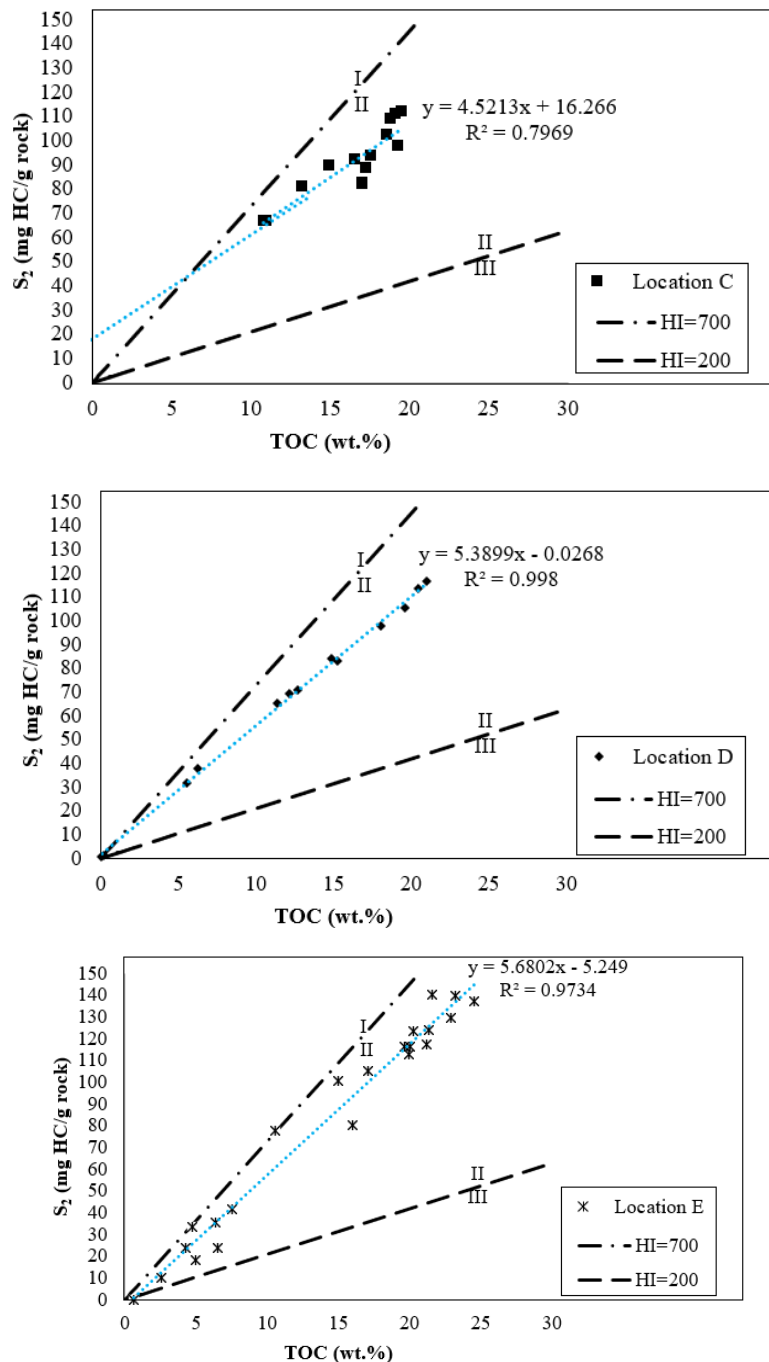


Figure 4

The HI versus TOC cross-plot, investigating the relationship between products and organic matter.





**Figure 5**

The S<sub>2</sub> versus TOC cross-plot, indicating y-intercept in locations A and C, showing bitumen contamination (Langford and Valleron, 1990).

Since the HI versus OI cross-plots (Figure 3) do not show the presence of inert kerogen but reveal the oil-prone kerogens, the x-intercept in the B, D, and E locations is created by the mineral matrix effect. Nevertheless, according to the regression line for all data plotted in Figure 5, the samples affected by the matrix effect are significantly lower than the contaminated samples. Furthermore, the two agents can be detected for creating that abnormal situation in the A and C locations; the first is the in situ bitumen contamination in the source rock, and the second is immigration to the source rock. According to Figure 6, the free hydrocarbons (S<sub>1</sub>) are indigenous and produced by the maturation of the organic

matter of the source rock, and no external agent, such as immigration, interfered in the contamination of the Garau formation (Espitalie et al., 1977; Hunt, 1996). The covalent bonding between hydrogen and carbon ions in the heavy bitumen of the Garau formation causes the generated products to adhere to the surface of organic facies. Then, the heavy bitumen remains in the source rock even at high temperatures and is not expelled quickly. Eventually, in situ contamination occurs (Morrison and Boyd, 1992; Mortimer, 1986).

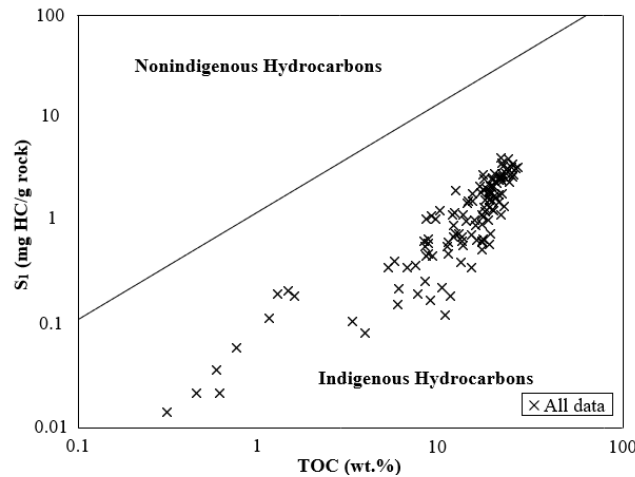


**Figure 6**

The  $S_1$  versus TOC cross-plot, finding out-migration from immigration (Hunt, 1996).

The calculated HI from contaminated samples by the Rock-Eval pyrolysis and without making any appropriate corrections usually do not represent the true HI. Such uncorrected data induce scattered plots and interception on the  $y$ -axis in the graphs of HI versus TOC and  $S_2$  versus TOC. The  $y$ -intercept, when induced, shows that the samples with high HI or  $S_2$  are associated with low TOC. The contamination causes the  $S_2$  and HI values to increase unrealistically and to decrease  $T_{max}$  from its actual values (Peters, 1986). In such situations, the thermal maturation occurs earlier, and the peak of  $S_2$  appears more easily. Then, the real thermal maturity in the contaminated samples is higher than the calculation with the Rock-Eval pyrolysis, and  $T_{max}$  cannot show an accurate thermal maturity level. According to the uncorrected  $T_{max}$  data from the Rock-Eval in locations A and C, the Garau formation is immature. However, the real maturity is higher in the mature stage.

The richness of the samples from organic carbon (high TOC) has led to the adsorption of heavy bitumen on organic matter-rich facies of the Garau formation. Subsequently, in situ contamination occurs, and the generated hydrocarbons are not expelled. Moreover, the diagram of the B, D, and E locations shows a slight  $x$ -intercept due to the mineral matrix effect (Langford and Valleron, 1990). After correcting the abovementioned formula, the actual geochemistry parameters are obtained and compared with calculated data from the Rock-Eval pyrolysis in Tables 2 and 3.

**Table 2**

The description of the kerogen type and measuring geochemistry parameters by the Rock-Eval pyrolysis.

Sampling location	Kerogen type	Mean HI mg HC/g TOC	Mean $S_2$ mg HC/gr rock	Mean $S_2/S_3$
Location A	I	588.0 (Range: 442–762)	91.7 (Range: 44.5–138.7)	92.9 (Range: 21.7–289.6)

Sampling location	Kerogen type	Mean HI mg HC/g TOC	Mean S <sub>2</sub> mg HC/gr rock	Mean S <sub>2</sub> /S <sub>3</sub>
Location B	I/II	449.3 (Range: 213–621)	38.4 (Range: 1.4–139.6)	30.6 (Range: 4.7–77.5)
Location C	I	555.2 (Range: 479–611)	90.5 (Range: 66–111.6)	61.9 (Range: 23.4–106.2)
Location D	II	478.7 (Range: 106–576)	67.0 (Range: 0.3–115.9)	61.9 (Range: 0.4–126.4)
Location E	I/II	497.0 (Range: 93–667)	82.6 (Range: 1.2–140.2)	73.2 (Range: 1.7–222.5)

**Table 3**

Actual geochemical parameters after correction.

Sampling location	Kerogen type	Mean HI mg HC/g TOC	Mean S <sub>2</sub> mg HC/gr rock	Mean S <sub>2</sub> /S <sub>3</sub>
Location A	I	484.11 (Range: 340–593.39)	77.00 (Range: 29.8–124)	78.07 (Range: 14.55–253.76)
Location B	I/II	583.58 (Range: 455.61–759.03)	40.30 (Range: 3.4–141.6)	34.45 (Range: 10.56–78.64)
Location C	I/II	452.52 (Range: 383–495.26)	74.3 (Range: 49.7–95.4)	50.81 (Range: 18.71–90.27)
Location D	I	479.59 (Range: 112.9–576.23)	67.0 (Range: 0.4–115.9)	61.87 (Range: 0.44–126.37)
Location E	I/II	561.97 (Range: 400.54–712.19)	87.9 (Range: 6.4–145.4)	77.74 (Range: 9.03–230.84)

On the basis of the cross-plots of S<sub>2</sub> versus TOC, the organic characteristics and hydrocarbon generation potential are almost similar in all locations. Regarding the geochemistry parameters of S<sub>2</sub>/S<sub>3</sub>, HI, and TOC, the Garau formation is predominantly considered a good-to-excellent source rock, which is formed mainly from kerogen type II, and some types I and III, with main expelled products of oil or gas mixed oil (Hunt, 1996; Jarvie, 1991).

## 5. Other applications

The cross-plots of S<sub>2</sub> versus TOC have been used to determine the depositional system tracts (Dahl et al., 2004; Maky et al., 2010; Phiri et al., 2014). The cross-plots of S<sub>2</sub> versus TOC are applied to determine the deposition environment of the rock samples. The current study's data are compared with the research of Robison and Engel (1993) about the usage of the cross plot of S<sub>2</sub> versus TOC in analyzing the transgressive system tracts (TST) and high-stand system tracts (HST) of the Late Cretaceous age in Egypt (Figure 7). The TST forms a smooth low angle (more considerable amounts of oil-prone organic carbon) close to a linear trend, while the HST forms a large and steeper angle (more gas-prone organic carbon) with a more chaotic distribution pattern. The TST is characterized by rising sea levels, lower terrestrial, and reworked organic matter (with higher HI values) entering the basin. Sediments are supplied chiefly from the basin. The HST is supported by the higher average amount of TOC, the low values of pyrolysable HI, and the scattered plot pattern suggesting that the organic material is derived from terrestrial and reworked materials that are typically gas-prone. In contrast, the TST is characterized by higher HI derived from higher TOC in a linear pattern. Hence, the clues prove that the Garau formation sedimented under anoxic conditions during sea level rise or transgression (Bordenave and Burwood, 1990; Haq et al., 1987; Sarfi et al., 2015).

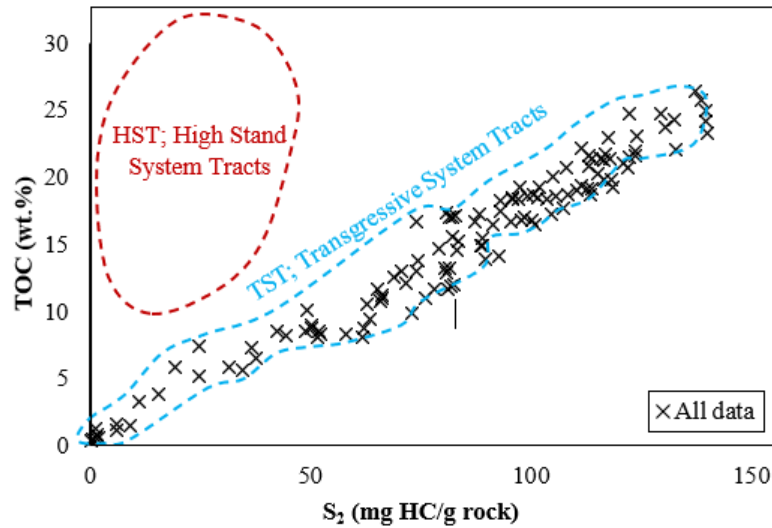


**Figure 7**

Characterization of sedimentary system tracts of Garau formation using  $S_2$  versus TOC parameters (modified after (Dahl et al., 2004; Robison and Engel, 1993)).

## 6. Conclusions

The adsorption of heavy bitumen to organic-rich facies prevents the easy expulsion of hydrocarbons and causes in situ bitumen contamination. The cross-plots of the  $S_2$  versus TOC are a criterion accuracy of geochemistry parameters and complement the Rock-Eval uncertainties. Accordingly, after drawing a regression line, the  $y$ -intercept is seen in the contaminated samples of two locations (A and C), which causes an overestimation in the  $S_2$  and HI values. The following formula is presented to eliminate the effect of contamination on the geochemistry parameters:

$$\text{Real } S_2 = S_2 - y_{\text{intercept}} \quad (7)$$

$$\text{Real HI} = \text{Real } S_2 / \text{TOC} \times 100 \quad (8)$$

$$\text{Real PI} = S_1 / S_1 + \text{Real } S_2 \quad (9)$$

In the three locations where the  $x$ -intercept is induced by the mineral matrix effect (B, D, and E), the real  $S_2$  is obtained according to the following formula:

$$\text{Real } S_2 = S_2 + y_{\text{intercept}} \quad (10)$$

Due to the effect of contamination and underestimation in the  $T_{\text{max}}$  values, this parameter could not be reliable for thermal maturity evaluations. Therefore, other parameters, such as vitrinite reflectance or biomarkers, should be applied to access thermal maturity.

Other applications of the  $S_2$  versus TOC graph include providing information on the depositional system tract. This method illustrates that the Garau formation is a type of HST system tract.

## Nomenclatures

HI	Hydrogen index, mg HC/gr TOC
HST	High-stand system tract
OI	Oxygen index, mg $\text{CO}_2$ /g TOC

PI	Production index, mg HC/g rock
TOC	Total organic carbon, wt %
TST	Transgressive system tract

## References

- Al-Husseini, and Moujahed I., Origin of the Arabian Plate structures: Amar collision and Najd rift, GEOARABIA-MANAMA, Vol. 5, No. 4, p. 527–542, 2000.
- Alavi, M., Regional stratigraphy of the Zagros fold-thrust belt of Iran and its proforeland evolution, *American Journal of Science*, Vol. 304, No. 1, p. 1–20, 2004.
- Bernard, Bernie B., Heather, B., and James, M., B., Determination of total carbon, total organic carbon and inorganic carbon in sediments, College Station, Texas, p. 1–5, 2010.
- Bordenave, M. L., and Burwood, R., Source rock distribution and maturation in the Zagros orogenic belt: provenance of the Asmari and Bangestan reservoir oil accumulations, *Organic Geochemistry*, Vol. 16, NO. 1, p. 369–387, 1990.
- Bordenave, M. L., and Hegre, J. A., Current distribution of oil and gas fields in the Zagros Fold Belt of Iran 424 and contiguous offshore as the result of the petroleum systems, *Geological Society, London, Special Publications*, Vol. 330, p. 291–353, 2010.
- Bordenave, M. L., and Hegre, J. A., The influence of tectonics on the entrapment of oil in the Dezful Embayment, Zagros Foldbelt, Iran, *Journal of Petroleum Geology*, Vol. 28, No. 4, p. 339–368, 2005.
- Bordenave, M. L., *Applied Petroleum Geochemistry*, Paris, Editions Technip, *Organic Geochemistry*, Vol. 21, p. 524, 1993.
- Clayton J. L., and Ryder, R. T., Organic geochemistry of black shales and oils in the Minnelusa Formation (Permian and Pennsylvanian), Powder River basin, Wyoming, In Woodward J, Meissner F. F, Clayton J. L. (Eds.), *Hydrocarbon source rocks of the greater rocky mountain region*, Denver, Rocky Mountain Association of Geologists, p. 231–253, 1984.
- Dahl, B., Bojesen-Koefoed, J., Holm, A., Justwan, H., Rasmussen, E., and Thomsen, E., A new approach to interpreting Rock-Eval S2 and TOC data for kerogen quality assessment, *Organic Geochemistry*, Vol. 35, No. 11–12, p. 1461–1477, 2004.
- Erik, N. Y., Özçelik, O., and Altunsoy, M., Interpreting Rock–Eval pyrolysis data using graphs of S2 vs. TOC: Middle Triassic–Lower Jurassic units, the eastern part of SE Turkey, *Journal of Petroleum Science and Engineering*, Vol. 53, No. 1–2, p. 34–46, 2006.
- Espitalie, J., Madec, M., Tissot, B., Menning, J. J., and Leplate, P., Source rock characterization on method for petroleum exploration, proceeding of the 9th Annual Offshore Technology Conference, Houston, p. 439–444, 1977.
- Espitalié, J., Deroo, G. and Marquis, F., La pyrolyse Rock-Eval et ses applications, partie II, *Revue de l'Institut français du Pétrole*, Vol. 40, No. 6, p. 755–784, 1985b.
- Espitalié, J., Deroo, G., and Marquis, F., La pyrolyse Rock-Eval et ses applications, partie I, *Revue de l'Institut français du Pétrole*, Vol. 40, No. 5, p. 563–579, 1985a.
- Ghazban F., and Motiei H., *Petroleum Geology of the Persian Gulf*, Tehran University and National Iranian Oil Company, Tehran, p. 722, 2007.

- Haq, B. U., Hardenbol, J. A. N., and Vail, P. R., Chronology of fluctuating sea levels since the Triassic, *Science*, Vol. 235, No. 4793, p. 1156–1167, 1987.
- Homke, S., Vergés, J., Serra-Kiel, J., Bernaola, G., Sharp, I., Garcés, M., Montero-Verdú, I., Karpuz, R. and Goodarzi, M.H., Late Cretaceous–Paleocene formation of the proto–Zagros foreland basin, Lurestan Province, SW Iran, *Geological Society of America Bulletin*, Vol. 121, No. 7–8, p. 963–978, 2009.
- Hunt, J. M., *Petroleum geochemistry and geology*, 2nd ed. W. H. Freeman and Company, New York, p. 743, 1996.
- Jarvie, D. M., Total organic carbon (TOC) analysis: Chapter 11: Geochemical methods and exploration, p. 113–118, 1991.
- Langford, F. F., and Blanc-Valleron, M. M., Interpreting Rock-Eval pyrolysis data using graphs of pyrolyzable hydrocarbons vs. total organic carbon (1), *AAPG Bulletin* Vol. 74, No. 6, p. 799–804, 1990.
- Maky, A. F., Ahmad, S., and Mousaand, N. I. M., Source rock and Paleoenvironmental evaluation of some pre-rift rock units at the Central part of the Gulf of Suez, Egypt. *J. Appl. Sci. Res*, Vol. 6, No. 5, p. 51, 2010.
- Miller, R. G., A future for exploration geochemistry, In Grimalt, J. O., Dorransoro, C. (Eds.), *Organic Geochemistry: Developments and Applications to Energy, Climate, Environment and Human History*, A.I.G.O.A., Donostia-San Sebastia´ N, Spain, p. 412–414, 1995.
- Morrison, R. T., and Boyd, R. N., *Organic Chemistry*, 6th ed, Prentice Hall, p. 1279, 1992.
- Mortimer, C. E., *General Chemistry*, 6th ed, Wadsworth Publishing Company, p. 902, 1986.
- Motiei, H., *Treatise on the geology of Iran: Stratigraphy of Zagros*, Geological Survey of Iran, Tehran, p. 497 (in Persian), 1993.
- Peters, K. E., and Cassa, M. R., Applied source rock geochemistry, In Magoon, L. B., Dow, W. G. (Eds.), *the Petroleum System—From Source to Trap*, AAPG, p. 93–120, 1994.
- Peters, K. E., and Fowler, M. G., Application of petroleum geochemistry to exploration and reservoir management, *Organic Geochemistry*, Vol. 33, p. 5–36, 2002.
- Peters, K. E., Guidelines for evaluating petroleum source rock using programmed pyrolysis, *Am. Assoc. Pet. Geol.*, Vol. 70, No. 3, p. 318–329, 1986.
- Phiri, C., Pujun, W. A. N. G., Nguimbi, G. R., and Hassan, A. Y. I., Interpreting effects of TOC inert organic content on source rock potential using S2 vs. TOC graph in Maamba Coalfield, southern Zambia, *Global Geology*, Vol. 17, No. 4, p. 199–205, 2014.
- Rimmer, S. M., Cantrell, D. J., and Gooding, P. J., Rock-Eval pyrolysis and vitrinite reflectance trends in the Cleveland Shale Member of the Ohio Shale, eastern Kentucky, *Organic Geochemistry*, Vol. 20, No. 6, p. 735–745, 1993.
- Robison, V. D., and Engel, M. H., Characterization of the Source Horizons within the Late Cretaceous Transgressive Sequence of Egypt, *AAPG Studies in Geology*, Vol. 37, p. 101–117, 1993.
- Sarfi, M., Ghasemi-Nejad, E., Mahanipour, A., Yazdi-Moghadam, M., and Sharifi, M., Integrated biostratigraphy and geochemistry of the lower Cretaceous Radiolarian Flood Zone of the base of the Garau Formation, northwest of Zagros Mountains, Iran, *Arabian Journal of Geosciences*, Vol. 8, No. 9, p. 7245–7255, 2015.

- Thomas, G. B., Weir, M. D., Hass, J., Heil, C., and Behn, A., *Thomas' Calculus: Early Transcendentals*, 13th edition, Boston, Pearson, 2016.
- Tissot, B. P., and Welte, D. H., *Petroleum formation and occurrence*. 2nd ed. Springer-Verlag Berlin Heidelberg, p. 702, 1984.
- Tyson, R.V., *Sedimentary Organic Matter: Organic Facies and Palynofacies*, Chapman and Hall, London, p. 615, 1995.
- Wynd, J. G., *Biofacies of the Iranian Consortium-agreement Area, Iranian Oil Operating Companies Report 1082 (Unpublished)*, 1965.



This article is an open-access article distributed under the terms and conditions of the Creative Commons Attribution 4.0 International (CC BY 4.0) (<https://creativecommons.org/licenses/by/4.0/>)